Null Flux Coils in Permanent Magnets Bearings

A. Musolino[1] , R. Rizzo[1] , L. Sani[1] and E. Tripodi[2]

[1]DESTEC, Department of Engineering for Energy and Systems Territory and Constructions, University of Pisa, Italy;
[2]Pure Power Control, Via Carbonia, 56021, Navacchio, Pisa, Italy

Abstract—**In this paper the stability analysis of a new Permanent Magnets (PMs) Bearings is presented and discussed. The suspension is assured by the repulsive force of properly shaped PMs placed on both the stator and the rotor. Then, exploiting currents induced on a system of null flux coils attached to the stator, a stabilizing force for the translation of the center of mass is obtained. The performance of the proposed bearing are investigated by a research code, previously developed at DESTEC and capable to simulate 6 DOF electromechanical devices.**

Index terms: **Computational electromagnetics, coupled analysis, eddy currents, electromechanical system, magnetic bearings.**

I. INTRODUCTION

The nowadays availability of rare heart Permanent Magnets (PMs), (e.g. NdFeB) characterized by high values of remnant field has made possible to conceive a new class of systems where the suspension is assured by the repulsion of properly shaped PMs [1] - [4]. An application example is flywheel energy storage systems, which are considered to be an attractive alternative to conventional electrochemical batteries [5], [6]. As known, stability of levitation for systems based on PMs only, is prevented by Earnshaw's theorem and Braunbeck's extension [7].

Anyhow, some circumstances exist in which electric and magnetic systems can avoid the theorem consequences, or at least mitigate the instability. For example, devices characterized by the presence of time-varying fields (e.g. eddy currents in alternating magnetic fields [8]- [13]) could not be affected by the instability problem. Other devices can be envisaged considering proper arrangements of PMs which are kept in motion nearby conductive domains. Under the correct conditions, the forces between the PMs and the motion induced eddy currents can be used to compensate the unstable forces between PMs [14]. Starting from this assumption it is possible to design permanent magnets-based systems which has evident advantages over existing ones.

The authors propose in the paper a device which can be considered a hybrid Magnetic Bearing (MB) combining Permanent Magnets MB with Electro-Dynamic Bearing (EDB). In the proposed device the PM provide an axial levitation, while the compensation of the radial instability of the PMs arrangement is provided by EDB. The stabilizing EDB is basically constituted by and array of Null Flux Coils (NFC). The proposed device was simulated by a 3D electromagnetic code coupled with the six degrees of freedom mechanical equations of the rigid body, to investigate its capability of reducing or eliminating the intrinsic instability of the magnetic bearings based on the PMs.

II. THE PROPOSED SYSTEMS

The proposed system is shown in figs. 1 and 2. It is composed of a toroidal stator and a segmented rotor made of (at least) three blocks equally spaced along the circumference. The stator is fixed while the rotor can move with 6 degrees of freedom (DOFs). The PMs in both the stator and the rotor are arranged in Halbach array configurations [15].
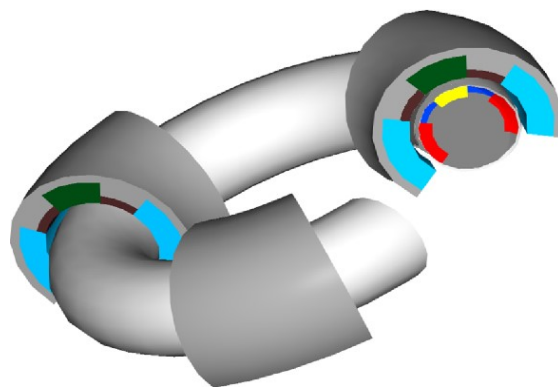
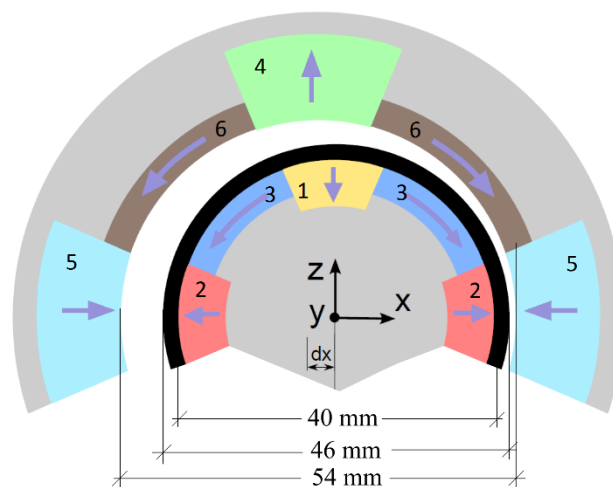

Fig. 1 A 3D view of the analyzed device
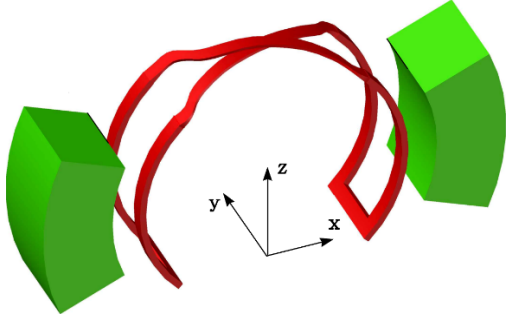

Fig. 2. Cross section of the bearing

Fig. 3 Interaction between a null-flux-coil and the lateral PMs (courtesy of [16]).

An array (in the azimuth direction) of null flux coils (see Fig. 3) surrounds the stator. The crossing of the conductors of the null flux coils is in correspondence of the central upper magnets, while the two halves of the coil face the lateral magnets of the rotor [16]. The region occupied by the null flux coils in evidenced in black in fig. 2. Levitation (along z-direction) is achieved by the repulsion of oppositely magnetized PMs.

In order to describe the dynamics of the proposed device let us first assume that the moving part rotates around a vertical shaft (directed as the z-axis) coincident with the symmetry axis of the stator. Corresponding to a clearance of 4 mm in the vertical (z-axis direction), the levitating force on the rotor is about 400N. The system is stable in the levitation direction since the levitation force is a decreasing function of the clearance variation w.r.t. its nominal value of 4mm. In all the dynamical simulation it is assumed that the bearing is loaded with a vertical force of 400N directed along the negative direction of the z-axis.

Let us consider the system rotating in its symmetric configuration: the rotation axis coincides with the symmetry axis of the rotor and with the symmetry axis of the stator. Because of the symmetry, the radial forces due to the interaction between the PMs have zero resultant. The electromotive force (e. m. f.) in every null flux is nearly zero. The magnetic drag force exerted by the NFCs on the PMs on the rotor is negligible and the radial force cancels.

If the symmetry condition does not hold (e.g. because of a radial shift of the rotation shaft) a net force in the radial direction is expected. This force is the resultant of the forces between the two PMs systems and of the forces between the motion induced currents in the null flux coils and the PMs on the rotor.

Considering the behavior of the arrangement of PMs only, we observe that, as a consequence of the Earnshow's theorem [7], when the rotor is given a lateral displacement (as in fig. 2, where the displacement is along the positive direction of the x-axis), the radial force has a non-zero resultant which has a component directed along the direction of the displacement.

If we consider the currents induced on the NFCs it is easy to see how they exert on the PMs on the rotor a resulting force which is directed along the negative x-axis direction so opposing to the force due to the interaction between the PMs [17], [18].

III. THE NUMERICAL CODE: SYNTHESIS

The system has been simulated by using a dedicated numerical code EN4EM (Electric Network for Electromagnetics), previously developed at University of Pisa for research purposes.

It is based on a 3D integral formulation it can simulate complex electromagnetic devices, transforming the solution of the field equations in the solution of an equivalent electric network [19], [20]. The code allows to obtain a set of equations that can be seen as the equilibrium equations set of an equivalent electric network. The currents in the branches of such auxiliary network are correlated with the currents in elementary volumes in which the devices are discretized. Then, the knowledge of these currents allows to evaluate all the electromagnetic quantities (fields, forces, eddy currents, and so forth) in the real devices.

The relative motion induced electromotive force is taken into account by the $v \times B$ term while the force on current carrying conductors is obtained by the $j \times B$ term. The formulation is here briefly summarized; the details are reported in [20].

Let us consider two bodies in relative motion and magnetically interacting (see fig. 4); they are discretized with n_1 and n_2 elementary volumes. A 3-D grid is obtained by connecting the centers of nearby elements. Subsequently a new elementary volume (evidenced in light red in the right portion of fig. 4) is associated to each segment of the grid.

These new elementary volumes carry uniformly distributed currents in the direction of the associated segment. Let N_1 and N_2 the numbers of conductive elements so obtained in the two bodies. Ohm's law is written at a point P inside the k-th elementary conductive volume:

$$\rho \boldsymbol{J}_k(P,t) = -\nabla V_k(P,t) - \frac{\partial}{\partial t} \boldsymbol{A}_k(P,t) + \boldsymbol{v}_k(P,t) \times \boldsymbol{B}_k(P,t) \quad (1)$$

where $\boldsymbol{J}_k(P,t)$ is the current density, $-\nabla V_k(P,t)$ is the irrotational component of the electric field, $\boldsymbol{A}_k(P,t)$ is the vector potential, ρ is the resistivity and $\boldsymbol{v}_k(P,t) \times \boldsymbol{B}_k(P,t)$ represents the motional term of the electric field.

By the additive property, we can write:

$$\rho \boldsymbol{J}_k(P,t) = -\nabla V_k(P,t) - \sum_{j=1}^{N_1+N_2} \frac{\partial}{\partial t} \boldsymbol{A}_{k,j}(P,t) + $$
$$ + \boldsymbol{v}_k(P,t) \times \sum_{j=N_1+1}^{N_2} \boldsymbol{B}_{k,j}(P,t) , 1 \le k \le N_1 \quad (2)$$

where $\boldsymbol{A}_{k,j}(P,t)$ and $\boldsymbol{B}_{k,j}(P,t)$ are respectively the vector potential and the magnetic flux density produced in P inside the k-th volume by the current in the j-th volume. Similarly when $N_1 + 1 \le k \le N_1 + N_2$.

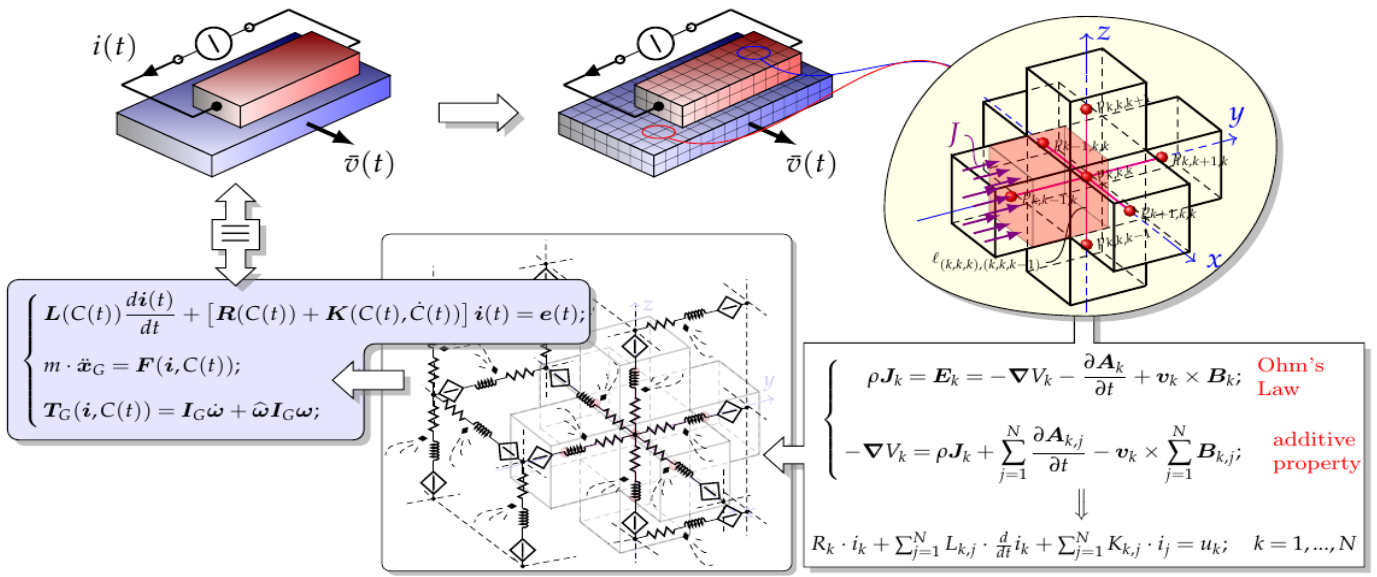The above equation is projected on the corresponding segment of the grid and is averaged on the cross section.

Fig. 4. Scheme of the numerical code.

It yields:

$$R_k i_k(t) + \sum_{j=1}^{N_1+N_2} L_{k,j}\frac{d}{dt}i_j(t) + \sum_{j=N_1+1}^{N_2} K_{k,j}i_j(t) = u_k(t),\ 1 \le k \le N_1$$

(3)

This is the governing equation of a branch, which is a series connection of a resistor, an inductor coupled with the inductors in the other branches and a controlled voltage generator which takes into account the motional effects. Connecting these branches the electric network reported in fig. 4 is obtained.

It is solved by the mesh analysis:

$$\boldsymbol{L}(\boldsymbol{C}(t))\frac{d\boldsymbol{i}(t)}{dt} + \left[\boldsymbol{R}(\boldsymbol{C}(t)) + \boldsymbol{K}(\boldsymbol{C}(t),\dot{\boldsymbol{C}})\right]\boldsymbol{i} = \boldsymbol{e}(t) \qquad (4)$$

where $\boldsymbol{i}$ is the vector of the currents on the chords and $\boldsymbol{e}$ is the vector of the imposed e.m.f. acting in the meshes. It is worth to note that some of the currents included in $\boldsymbol{i}$ may be imposed. In particular the imposed current can represent the equivalent magnetization currents of the PMs. Because of the relative movement, some of the elements of the matrices $\boldsymbol{L}(\boldsymbol{C}(t))$ and $\boldsymbol{K}(\boldsymbol{C}(t),\dot{\boldsymbol{C}})$ change and have to be evaluated at every time. $\boldsymbol{C}(t)$ is a vector including the set of positions and orientations of the elementary volume at the instant t and $\dot{\boldsymbol{C}}$ is its derivative. Once the currents are evaluated, the force on the k-th volume due to current on the j-th elements is written as:

$$\boldsymbol{f}_{jk} = \int_{\Gamma_k} \boldsymbol{j}_k \times \boldsymbol{B}_{k,j}\, d\Gamma \qquad (5)$$

where $\boldsymbol{j}_k$ is the current density and the and $\boldsymbol{B}_{k,j}$ is the flux density in the k-th volume produced by the current flowing in the j-th one. Finally electrical equations are coupled with the rigid body mechanical equation:

$$m \cdot \ddot{\boldsymbol{x}} \quad \boldsymbol{F}\ \boldsymbol{i}, \boldsymbol{C}(t))$$

$$\boldsymbol{T}_G(\boldsymbol{i}, \boldsymbol{C}(t)) = \boldsymbol{I}_G\dot{\boldsymbol{\omega}}\quad \boldsymbol{\omega}\quad \boldsymbol{I}\ \boldsymbol{\omega}$$

Where $\boldsymbol{x}_G$ represents the center of mass of the rotor, $\boldsymbol{F}$ is the resultant of the forces, $\boldsymbol{I}_G$ is the tensor of inertia and $\boldsymbol{T}_G$ is the resultant of the torques; both are referred to the center of mass of the rotor. Since the differential equations for the electrical and dynamic equilibrium are coupled, the resulting system is time varying; the equations are integrated by using a recently proposed predictor-corrector [19].
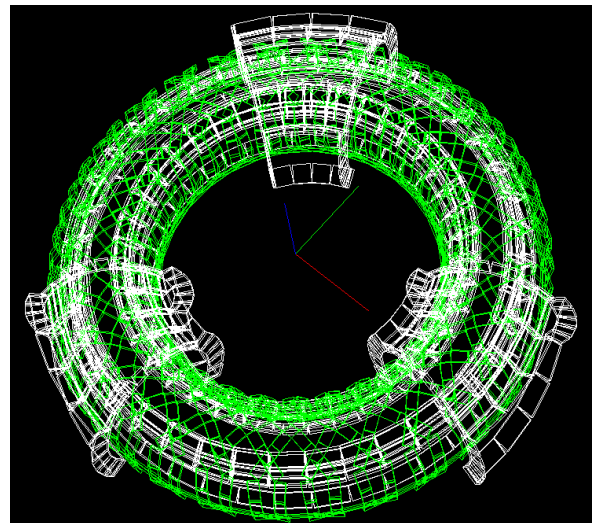

Fig. 5. The mesh used by EN4EM to simulate the whole system.

The solution of the model allows to know all the electromagnetic and mechanical quantities which govern the operation of a given 6 DOF device. The geometry of the device is here described with reference to fig. 2 which is not in scale. The major radius of the torus is 80 mm; the minor radius of the stator is 20 mm; the inner radius of the rotor is 2.7 mm; the conductive material (copper continuous sheet of array of copper made NFCs) attached to the stator has a thickness of 3mm; the clearance between stator and rotor is then 4 mm. The magnet on the stator labelled with 1 in fig. 2, spans an angle of 45 degree in the poloidal direction and is 6 mm thick in the direction of the minor radius. The magnets labelled with 2 span angles of 67.5 degree with the same thickness as the number 1. The magnets labelled with 3 span 33.75 each and are 4 mm thick. The rotor is constituted by three equally spaced segments which span 45 degree each in the toroidal direction. The magnets number 4, 5 and 6 span the same angle in the poloidal direction as 1, 2 and 3 respectively. The thickness of 4 and 5 is 8 mm, while the thickness of magnets labelled with 6 is 3 mm. The direction of the magnetization is reported in fig. 2. A linear characteristic is assumed for the PMs with a remnant magnetization of $B_r = 1.02\ T$ and μ_0 as the magnetic permeability.

Figure 5 shows the discretization used by the numerical code to simulate the proposed device. The circular array of 30 null flux coils, partially overlapping, is shown in green color. The PMs in both the stator and the rotor are modeled by using a system of equivalent surface currents and are shown in white.

A number of simulation has been performed on the described system in order to investigate the effectiveness of the null flux coils in the stabilization of the device. The results are shown in the next section.

IV. THE RESULTS

A first characterization of the proposed bearing has been performed when the rotor is at rest considering different values of eccentricity and vertical position of the rotor with respect to the stator. Since the system is stable in the vertical direction, it is unstable in the lateral direction (Earnshaw's and Braunbeck's theorems) as confirmed by the following figures. In particular, fig. 6 reports the vertical (levitating) force on the rotor as a function of the clearance between the rotor and the upper portion of the null lux coils in the range [0, 6mm], for different values of lateral (x-axis) displacement in the range [0, 4mm]. The negative slope of the curves confirms the stability along the vertical axis.

Figure 7 reports the lateral (x-axis) force on the rotor as a function of the lateral displacement for different values of the clearance between stator and rotor. The slope of the curves is positive, and this confirm the unstable behavior along the horizontal direction. These figure shows that in the considered ranges of lateral and axial displacement the proposed bearing has a ratio F_z/F_x typically greater than 20.
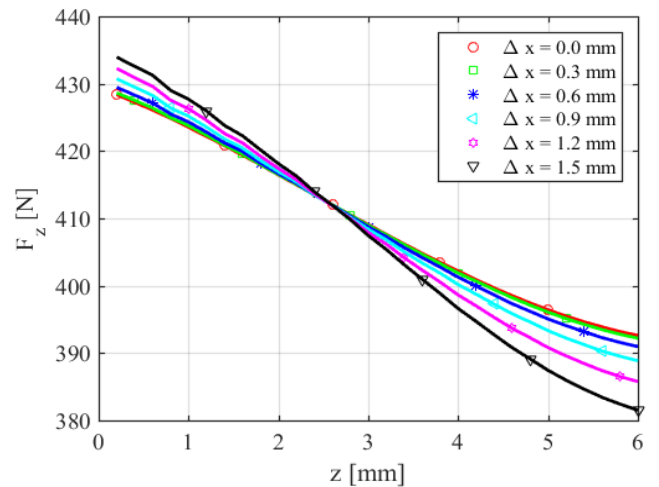

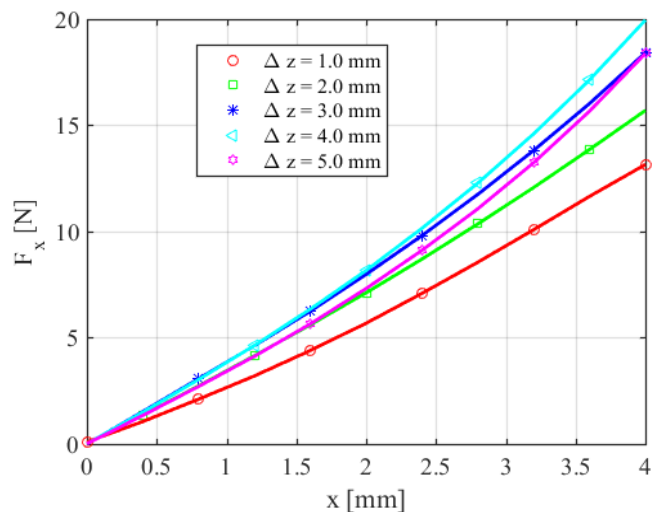Fig. 6. Levitating force as function of the vertical clearance.

Fig. 7. Lateral force as a function of the displacement from coaxial condition.

We carried out some simulations to investigate the possibility of stabilizing in a totally passive manner the proposed bearing. In particular we investigate the ability of the device to recover the initial equilibrium configuration when it starts from a perturbed position. The equilibrium configuration under the vertical load of 400 N is the one corresponding to a concentric geometry in fig.2, i.e. the symmetry axes of stator and rotor are coincident and also correspond to the rotation axis. The initially perturbed configuration is obtained by the one above described by shifting the rotation axis (coincident with the symmetry axis of the rotor) of a displacement $dx=1.5mm$ along the x-axis positive direction.

We considered an array of 30 NFCs equally spaced in the toroidal direction. The cross section of the conductor (copper) is a rectangle with sides: 3 mm in radial direction and 4mm in the

toroidal one. The length of the coil in the toroidal direction is 35 mm, which is approximately the 65% of the magnets length as recommended in [18].

Fig.s 8 and 9 respectively show the x and y components of the velocity of the center of mass of the rotor in correspondence of some rotation speeds and for the given initial displacement.

Figs. 10 and 11 respectively show the x and y components of the rotational velocity of the rotor with respect to center of mass for the same initial lateral displacement. The end of each curve coincides with the instant when the rotor collapses on the stator. We see that the rotation speed characterized by the slowest instability is $\Omega = 500 \; rad/s$.

In [20] the authors have analyzed the behavior of a similar device rotating at $\Omega = 500 \; rad/s$ (the arrangement of the PMs is the same, as well as the initial configuration, and a continuous conductive sheet substitutes the array of null flux coils). The results obtained are here reported in figs. 12 and 13.
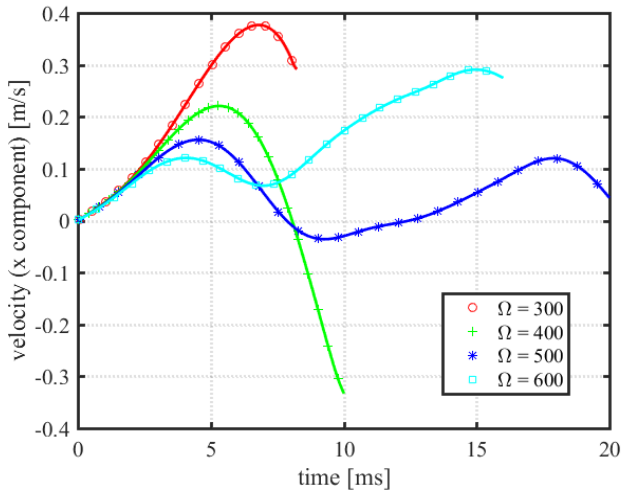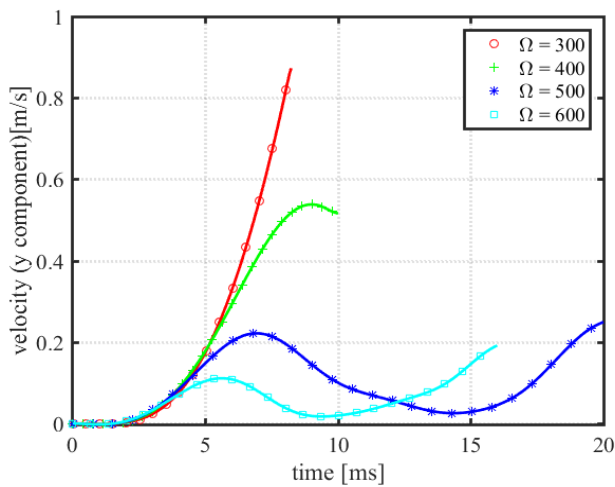
Fig. 9. y axis component of the velocity of the center of mass.

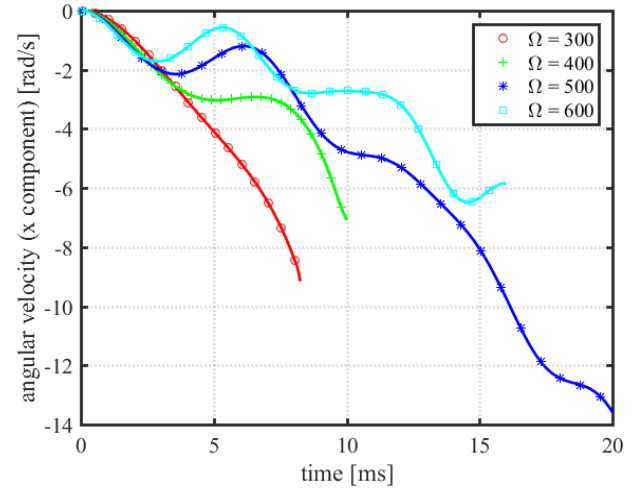Fig. 10. x axis component of the angular velocity w.r.t. the center of mass.

Fig. 8. x axis component of the velocity of the center of mass.
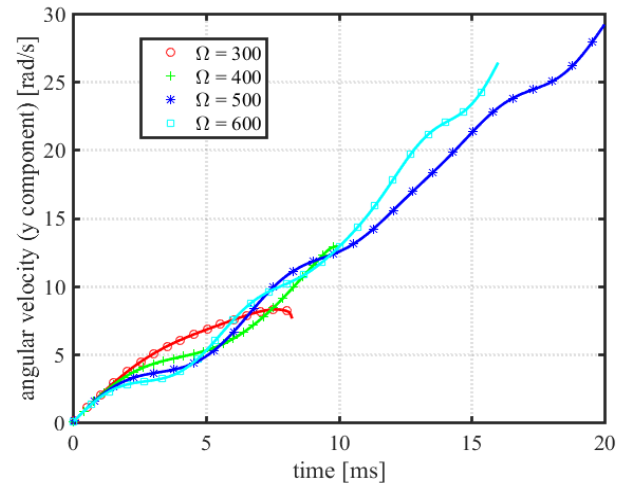

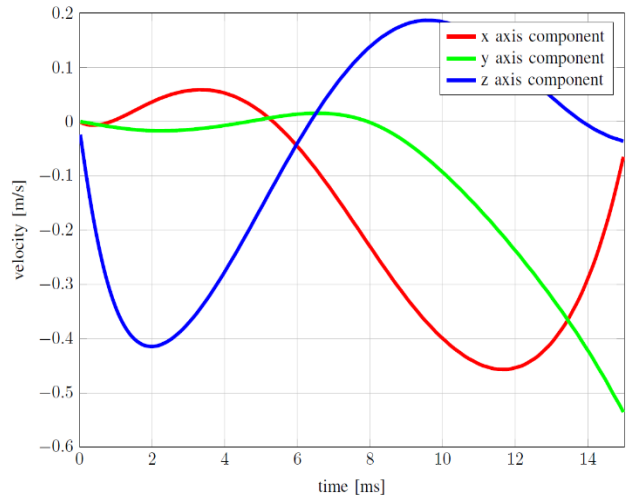Fig. 11. y axis component of the angular velocity w.r.t. the center of mass.

Fig. 12. Component of the velocity of the center of mass with the continuous

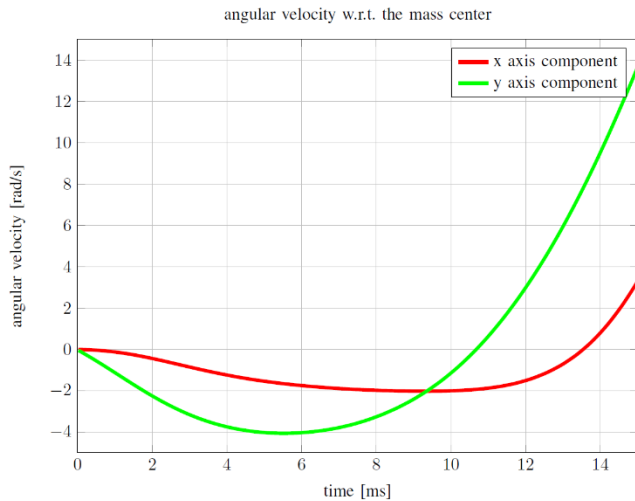conductive sheet at the rotation speed of 500 rpm (courtesy of [20]).

Fig. 13. Component of the x and y components of the angular velocity with the continuous conductive sheet at the rotation speed of 500 rpm (courtesy of [20]).

Comparison of the reported waveforms shows a better performance of the null flux coils over the continuous conductive sheet.

A deeper analysis of the waveforms shows that the velocity of the center of mass benefits from the presence of the null flux coils. The same is not true about the transverse components of the angular velocity, since the main effect of the adopted null flux coils configuration is to contrast the transverse displacement of the rotation axis, and not its tilt.

Another factor that makes the NFCs more attractive with respect to the continuous sheet is the reduced magnetic drag torque. This is clearly shown by fig. 14 which reports the comparison between the drag torques for the two configurations.
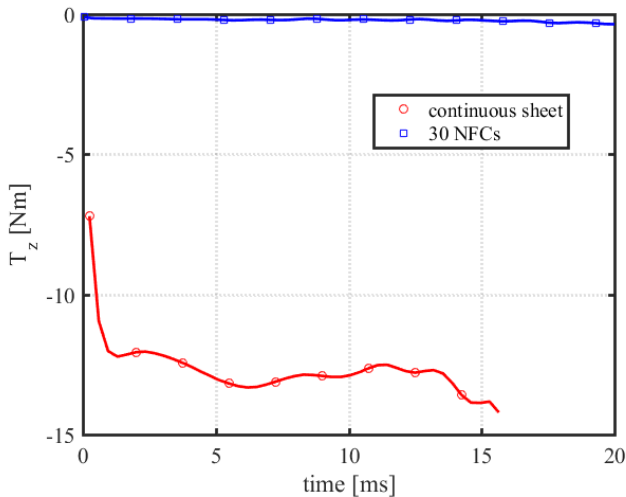
In both the configurations the eddy currents induced in the PMs were discarded (the conductivity of the PMs was zero). Considering the typical values of the conductivity of PMs, which is about two magnitude order lower than that of aluminum or copper, from a rough comparison of the results obtained with the continuous conductive sheet, we can reasonably assume that the drag torque due to the eddy currents in the PMs is at least two order of magnitude less than that due to the continuous sheet. Considering also that the magnet on the stator are segmented this should further reduce the effects of the induced eddy currents on the PMs.

The performance of the null flux coils in contrasting the lateral instability have been investigated by reducing to four the number of degrees of freedom of the rotor preventing the tilt of the shaft.

We analyzed two arrangements of null flux coils characterized by the presence of 30 and 40 identical null flux coils equally spaced on the stator similar to the ones previously described We performed several simulations at different rotation speeds, reporting the components of the velocity on the rotor in the x and y directions as well the forces on the rotor.

Figures 15 and 16 report the components of the lateral force on the rotor when 30 null flux coils are present on the stator for different speeds.

As shown by the figures, the device shows a pronounced lateral instability at $\Omega = 300\ rad/s$ and $\Omega = 400\ rad/s$; the instability is substantially reduced at $\Omega = 500\ rad/s$. The simulations at $\Omega = 600\ rad/s$ show that the behavior is stable, although not asymptotically, since both the component of the force approach an oscillating behavior with a constant amplitude.

Fig. 14. Comparison of the drag torque between the continuous conductive sheet and the NFCs at the rotation speed of 500 rpm.
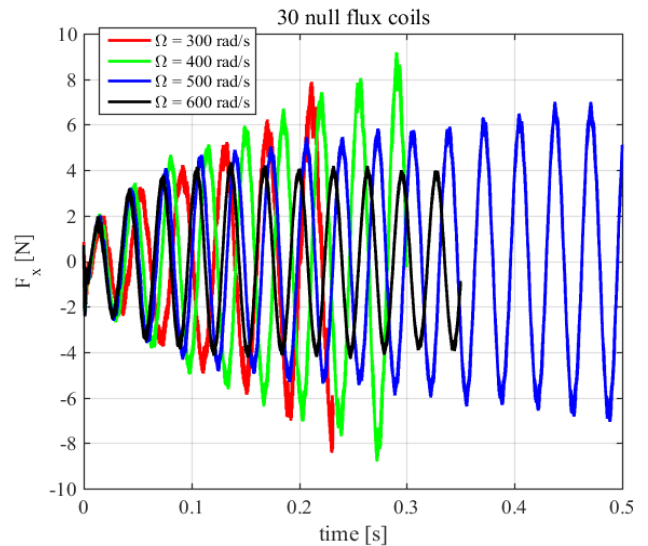

Fig. 15. x-axis component of the force on the rotor when 30 null flux coils are on
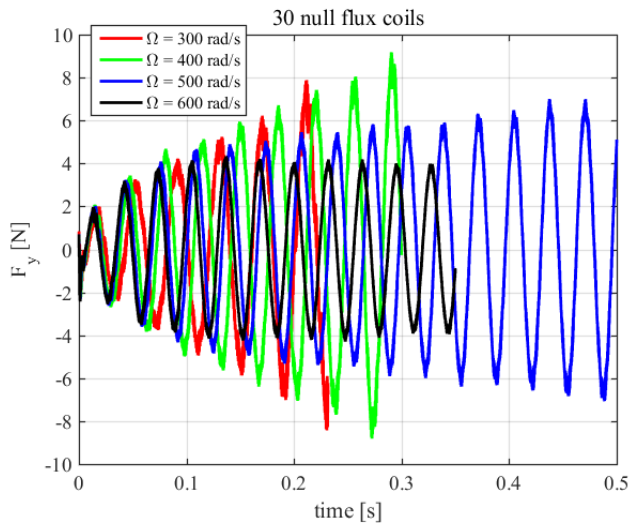
the stator.

Fig. 16. y-axis component of the force on the rotor when 30 null flux coils are on the stator.
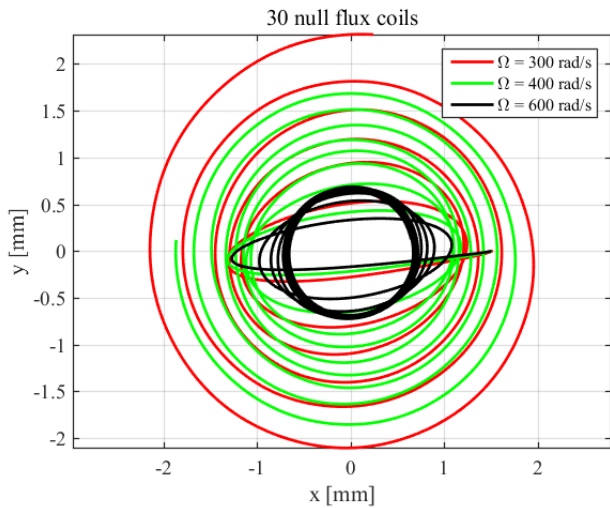

Fig. 17. Trajectory of the center of the shaft of the rotor when 30 null flux coils are on the stator. The orbit is travelled in the clockwise direction.

This is well evidenced in fig. 17 which shows the trajectory of the center of the shaft in the *x-y* plane.

Figures 18 and 19 show the component of the force on the rotor when the number of null flux coils on the stator is 40. In this case the system is stable for every angular speed in the considered range. This behavior is confirmed by the trajectories of the center of the shaft as shown in fig. 20.

The thickness of the lines which represent the forces is due to a ripple produced by the discrete distribution of the conductors on the stator. When flux lines of the magnets on the rotor enter a null flux coil the induced currents start producing a force which sums up with the forces due to the other null flux coils. Similarly when a magnet leaves a null flux coil. Considering the number

of null flux coils, the fundamental harmonic component of the ripple on the force is 30 or 40 times the angular speed of the rotor and cannot be seen on the figures which report simulated times of the order of tenths of second.

The described simulations show that a minimum angular speed and a minimum number of NFCs distributed along the torus are needed to compensate for the lateral instability. Another interesting result is the absence of rotor-dynamic instabilities which can affect the electrodynamic bearing. This drawback has been observed and discussed the literature. A detailed analysis is reported in [12], where the introduction of a proper damping is proposed to stabilize the device. The arrangement of NFCs proposed in the paper is free of this drawback.
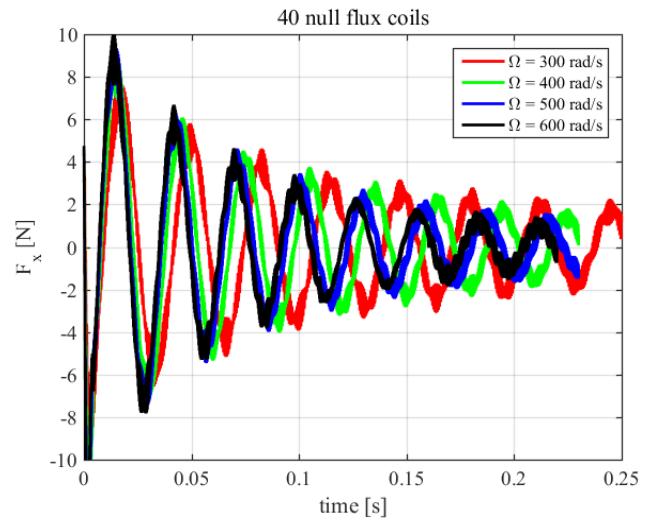

Fig. 18. x-axis component of the force on the rotor when 40 null flux coils are on the stator.
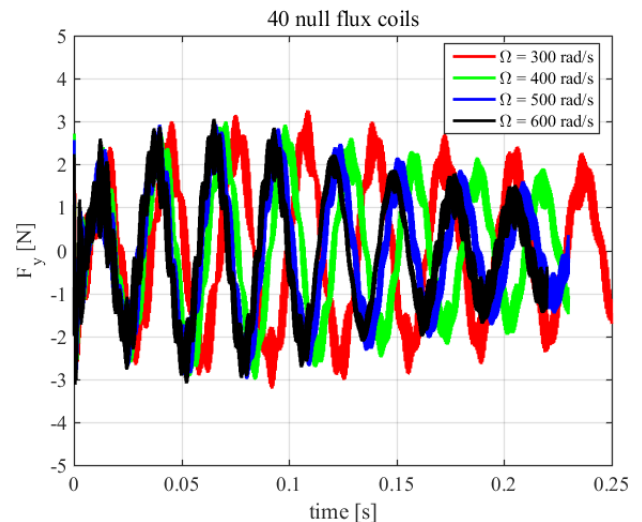

Fig. 19. y-axis component of the force on the rotor when 40 null flux coils are on the stator.
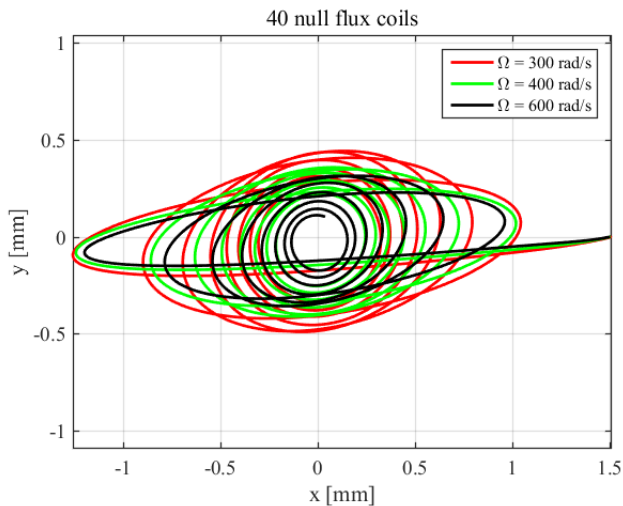
Fig. 20. Trajectory of the center of the shaft of the rotor when 30 null flux coils are on the stator. The orbit is travelled in the clockwise direction

V. CONCLUSION

A preliminary coupled electromechanical analysis of a passively stabilized magnetic bearing device has been presented. The results of the numerical simulations performed on two configurations of the proposed system has shown the effectiveness of the motion induced currents as a tool for the dynamic stabilization of the center of mass. Stabilization is obtained with respect to deviation from the equilibrium position. Because of this behavior, the active stabilization devices, if needed, have to compensate the instabilities with respect to the rotations only. If the stabilizing forces have a non-zero resultant, the system is able to compensate it. This makes simpler the design and the operation of the active stabilization devices.

ACKNOWLEDGMENT

REFERENCES

[1] R. Skomski, P. Manchanda, P. Kumar, B. Balamurugan, A. Kashyap, and D. J. Sellmyer, "Predicting the future of permanent-magnet materials," *IEEE Trans. Magn.*, vol. 49, no. 7, pp. 3215-3220, Jul. 2013.
[2] E. Cardelli, E. Della Torre, A. Faba, " Numerical Modeling of Hysteresis in Si-Fe Steels", IEEE Transactions on Magnetics, VOL. 50, NO. 2, February 2014.
[3] E. Cardelli, A. Faba, " Modeling of hysteresis in magnetic multidomains", Physica B: Condensed Matter, Vol. 435, p. 62–65, February 2014.
[4] S. I. Bekinal, T. R. Anil, and S. Jana, "Analysis of axially magnetized permanent magnet bearing characteristics," *Progress In Electromagnetics Research B*, vol. 44, pp. 327-343, 2012.
[5] M. Ceraolo, G. Lutzemberger, D. Poli: "Aging evaluation of high power lithium cells subjected to micro-cycles", *Journal of Energy Storage*, vol. 6, pp.: 116-124, 2016.
[6] S. Barsali, M. Ceraolo, R,Giglioli, D. Poli, "Storage applications for smartgrids", *Electric Power System Research (EPSR)*, vol. 120, pp.: 109-117, Mar. 2015.
[7] W. Braunbek, "Freischwebende korper in elektishen und magnetishen feld*," Z. Phisik*, vol. 112, pp. 753-763, 1939.
[8] Detoni, J.G., Cui, Q., Amati, N., Tonoli, A., "Modeling and evaluation of damping coefficient of eddy current dampers in rotordynamic applications", Journal of Sound and Vibration, Vol. 373, pp. 52-65, 2016.
[9] Impinna, F., Detoni, J.G. , Amati, N., Tonoli, A., "Passive magnetic levitation of rotors on axial electrodynamic bearings", IEEE Trans. on Mag., Vol. 49, n. 1, pp. 599-608, 2013.
[10] A. V. Filatov, E. H. Maslen, "Passive magnetic bearing for flywheel energy storage systems," *IEEE Trans. Magn.*, vol. 37, no. 6, pp. 3913-3924, 2001.
[11] C. Dumont, V. Kluyskens, B. Dehez, "Linear state-space representation of heteropolar electrodynamic bearings with radial magnetic field", *IEEE Trans. Magn.*, vol. 52, no. 1, pp. 1-9, 2016.
[12] A. Tonoli, N. Amati, F. Impinna, & J. G. Detoni. "A solution for the stabilization of electrodynamic bearings: Modeling and experimental validation" *Journal of Vibration and Acoustics*, vol. 133, n. 22, 2011.
[13] A. Filatov, E. H. Maslen, and G. T. Gillies. "Stability of an electrodynamic suspension." *J. of App. Phys*. vol. 92, no. 6, pp. 3345-3353, 2002.
[14] N. Paudel, S. Paul, and J. Z. Bird, "General 2-D transient eddy current force equations for a magnetic source moving above a conductive plate," *Progress In Electromagnetics Research B*, vol. 43, pp. 255-277, 2012.
[15] R. Ravaud, G. Lemarquand, and V. Lemarquand, "Halbach structures for permanent magnets bearings," *Progress In Electromagnetic Research M*, vol. 14, pp. 263-277, 2010.
[16] A. Musolino, M. Raugi, R. Rizzo, E. Tripodi, "Stabilization of a permanent-magnet MAGLEV system via null-flux coils," *IEEE Trans Plasma Sci.* vol. 43, no. 5, pp.: 1242-1247, May, 2015.
[17] J. de Boeij, M. Steinbuch, H.M. Gutierrez, "Modeling the electromechanical interactions in a null-flux electrodynamic maglev system," ," *IEEE Trans. Magn,* vol. 41, no. 1, pp.: 466-470, Jan. 2005.
[18] K. R. Davey, "Designing with null flux coils," *IEEE Trans. Magn,* vol. 33, no. 5, pp.: 4327-4334, Sept. 1977.
[19] E. Tripodi, A. Musolino, M. Raugi and R. Rizzo," A new predictor-corrector approach for the numerical integration of coupled electromechanical equations" *Int, J. on Num Meth. Eng,*vol. 105, no. 4, pp. 261-285, 2016.
[20] A. Musolino, R. Rizzo, M. Toni and E. Tripodi, "Modeling of electromechanical devices by GPU-accelerated integral formulation," *Int. J. of Num. Modeling: Electron. Networks, Devices and Fields*, vol. 26, no. 4, pp. 373-396, 2013.